the harmonic frequency 25 Hz. Hence, variable holding times in the trap translate into variable initial velocities during application of the subsequent heating pulse, provided that the pulse duration (400 μs) is much shorter than the oscillation period of about 40 ms. Because the initial velocity Doppler-shifts the backscattering resonances in Fig. 1, B and C, the populations P_n of the momentum components $n2\hbar k$, $n \in \{0, -1, 1\}$ are expected to vary periodically with the holding time. This is illustrated in Fig. 4A, where momentum spectra are shown that were recorded after application of an excitation pulse similar as in Fig. 3A following a variable holding time in the magnetic trap. The lines in Fig. 4B show the quantities $\pi_0 = P_0/(P_0 + P_{-1} + P_1)$ (blue) and $\pi_1 = (P_1 - P_{-1})/(P_0 + P_{-1} + P_1)$ (red), which have been calculated by using Eqs. 1 and 2 with $q(t) = q_0\cos(\Omega t)$ and $q_0 \approx 0.1k$ determined by a time-of-flight measurement. The fine details of these traces largely depend on the exact values of the pulse durations, detunings, and powers. Nevertheless, the coarse structure describes well the observations in Fig. 4A (*25*).

Cavity-induced sub-recoil momentum transfer could be used to also cool hotter, truly thermal samples by applying sequences of pulses with appropriately adjusted frequency detunings. Cross-dimensional relaxation because of ergodic mixing in the external potential and elastic collisions should allow us to cool all three dimensions. The achievement of quantum degeneracy starting from a thermal sample well above the critical temperature is an intriguing goal, which appears to be in reach with our cooling scenario.

References and Notes

1. C. Adams, E. Riis, *Prog. Quantum Electron.* **21**, 1 (1997).
2. H. Metcalf, P. van der Straten, *Laser Cooling and Trapping* (Springer, New York, 1999).
3. T. Udem, R. Holzwarth, T. W. Hänsch, *Nature* **415**, 233 (2002).
4. S. A. Diddams, J. C. Bergquist, S. R. Jefferts, C. W. Oates, *Science* **306**, 1318 (2004).
5. I. Bloch, J. Dalibard, W. Zwerger, *Rev. Mod. Phys.* **80**, 885 (2008).
6. P. Horak, G. Hechenblaikner, K. M. Gheri, H. Stecher, H. Ritsch, *Phys. Rev. Lett.* **79**, 4974 (1997).
7. V. Vuletić, S. Chu, *Phys. Rev. Lett.* **84**, 3787 (2000).
8. P. Domokos, H. Ritsch, *J. Opt. Soc. Am. B* **20**, 1098 (2003).
9. P. Maunz *et al.*, *Nature* **428**, 50 (2004).
10. S. Nußmann *et al.*, *Nat. Phys.* **1**, 122 (2005).
11. A. Beige, P. L. Knight, G. Vitiello, *New J. Phys.* **7**, 96 (2005).
12. G. Morigi, P. W. H. Pinkse, M. Kowalewski, R. de Vivie-Riedle, *Phys. Rev. Lett.* **99**, 073001 (2007).
13. D. R. Leibrandt, J. Labaziewicz, V. Vuletić, I. L. Chuang, *Phys. Rev. Lett.* **103**, 103001 (2009).
14. T. J. Kippenberg, K. J. Vahala, *Science* **321**, 1172 (2008).
15. E. M. Purcell, H. Torrey, R. Pound, *Phys. Rev.* **69**, 37 (1946).
16. H. W. Chan, A. T. Black, V. Vuletić, *Phys. Rev. Lett.* **90**, 063003 (2003).
17. A. T. Black, H. W. Chan, V. Vuletić, *Phys. Rev. Lett.* **91**, 203001 (2003).
18. K. W. Murch, K. L. Moore, S. Gupta, D. M. Stamper-Kurn, *Nat. Phys.* **4**, 561 (2008).
19. F. Brennecke, S. Ritter, T. Donner, T. Esslinger, *Science* **322**, 235 (2008); 10.1126/science.1163218.
20. T. P. Purdy *et al.*, *Phys. Rev. Lett.* **105**, 133602 (2010).
21. K. Baumann, C. Guerlin, F. Brennecke, T. Esslinger, *Nature* **464**, 1301 (2010).
22. S. Slama, S. Bux, G. Krenz, C. Zimmermann, P. W. Courteille, *Phys. Rev. Lett.* **98**, 053603 (2007).
23. S. Bux, C. Gnahm, R. A. W. Maier, C. Zimmermann, P. W. Courteille, *Phys. Rev. Lett.* **106**, 203601 (2011).
24. B. Nagorny *et al.*, *Phys. Rev. A* **67**, 031401 (2003).
25. Supplementary materials are available on *Science* Online.
26. P. Horak, S. M. Barnett, H. Ritsch, *Phys. Rev. A* **61**, 033609 (2000).

Acknowledgments: This work was partially supported by Deutsche Forschungsgemeinschaft (He2334/12-1, SFB 925, GrK 1355) and the Excellence cluster "Frontiers in Quantum Photon Science." A.H. is grateful to E. Demler, L. Mathey, and C. Morais Smith for useful discussions.

Supplementary Materials

www.sciencemag.org/cgi/content/full/337/6090/75/DC1
Materials and Methods
References (*27*–*29*)

16 January 2012; accepted 8 May 2012
10.1126/science.1219166

Large Volcanic Aerosol Load in the Stratosphere Linked to Asian Monsoon Transport

Adam E. Bourassa,[1]* Alan Robock,[2] William J. Randel,[3] Terry Deshler,[4] Landon A. Rieger,[1] Nicholas D. Lloyd,[1] E. J. (Ted) Llewellyn,[1] Douglas A. Degenstein[1]

The Nabro stratovolcano in Eritrea, northeastern Africa, erupted on 13 June 2011, injecting approximately 1.3 teragrams of sulfur dioxide (SO_2) to altitudes of 9 to 14 kilometers in the upper troposphere, which resulted in a large aerosol enhancement in the stratosphere. The SO_2 was lofted into the lower stratosphere by deep convection and the circulation associated with the Asian summer monsoon while gradually converting to sulfate aerosol. This demonstrates that to affect climate, volcanic eruptions need not be strong enough to inject sulfur directly to the stratosphere.

Aerosols in the stratosphere have an important influence on climate variability: They scatter incident sunlight, thus cooling Earth's surface, but with a highly variable effect owing to the size and frequency of volcanic eruptions. Sustained aerosol concentrations in the stratosphere are supported by particles with lifetimes of a year or longer, mainly sub-micrometer hydrated sulfuric acid droplets rather than solid particles, such as volcanic ash, which due to their size settle from the stratosphere more quickly. Sulfuric acid droplets form at stratospheric altitudes through oxidation of gases containing sulfur, mainly carbonyl sulfide and sulfur dioxide (SO_2) (*1*). For a volcanic eruption to affect stratospheric aerosol substantially, it typically has to be sulfur-rich and energetic enough to penetrate the tropopause. The Nabro stratovolcano in Eritrea, northeastern Africa, erupted on 13 June 2011, with ash clouds reaching altitudes of 9.1 to 13.7 km (*2*). Nadir measurements made by the Ozone Monitoring Instrument (OMI) show that the total emitted SO_2 was approximately 1.3 Tg (*3*). These reported eruption heights are below tropical tropopause levels, which are 16 km or higher. In spite of this, scattered sunlight measurements from the limb-scanning Optical Spectrograph and Infra-Red Imaging System (OSIRIS) satellite instrument (*4*) show that Nabro caused the largest stratospheric aerosol load in the decade-long OSIRIS measurement record. Additionally, the OSIRIS measurements show the aerosol enhancement building most strongly above the Asian monsoon, which has recently been identified as a potentially effective pathway for transport of air from the troposphere to the stratosphere (*5*) and a potentially important region for the formation of small stratospheric aerosol particles during volcanically unperturbed conditions (*6*, *7*).

Global measurements of the stratospheric aerosol load have been made by limb-scanning solar occultation satellite instruments for decades. These aerosol extinction measurements, in particular from the Stratospheric Aerosol and Gas Experiment (SAGE) series of instruments (SAGE, 1979 to 1981; SAGE II, 1984 to 2005; and SAGE III, 2002 to 2005), have provided an essential understanding of the stratospheric aerosol layer. SAGE II measurements were especially important for tracking and quantifying the eruptions of El Chichón in 1982 (*8*) and Mount Pinatubo in 1991 (*9*, *10*), both of which caused

[1]Institute of Space and Atmospheric Studies, University of Saskatchewan, Saskatoon, SK S7N 5E2, Canada. [2]Department of Environmental Sciences, Rutgers University, New Brunswick, NJ 08901, USA. [3]National Center for Atmospheric Research, Boulder, CO 80307, USA. [4]Department of Atmospheric Science, University of Wyoming, Laramie, WY 82071, USA.

*To whom correspondence should be sent. E-mail: adam.bourassa@usask.ca

considerable cooling of the lower troposphere in the 2 years after the eruption (*11*, *12*).

Since the eruption of Mount Pinatubo in 1991, there have been no major volcanic eruptions that have substantially increased the stratospheric aerosol load. However, in the past decade an increase in the so-called "background" level has been observed. Ground-based lidar measurements show that the stratospheric aerosol load has increased since 2000 at 5 to 7% per year (*6*). Suggested causes of this increase range from increased anthropogenic emissions (*6*) to variability associated with a series of small, typically tropical, volcanic eruptions (*13*). This "persistently variable" increase in the background level has been shown to cause an additional radiative forcing of –0.1 W/m^2 over the past decade, effectively reducing the impact of greenhouse gas increases over the same time period (*14*). The effects of these relatively minor eruptions are important to include for climate model predictions in order to avoid overestimation of radiative forcing and thus global warming. The effect of the 2011 Nabro eruption will extend the negative forcing from the stratospheric aerosol changes observed over the past decade.

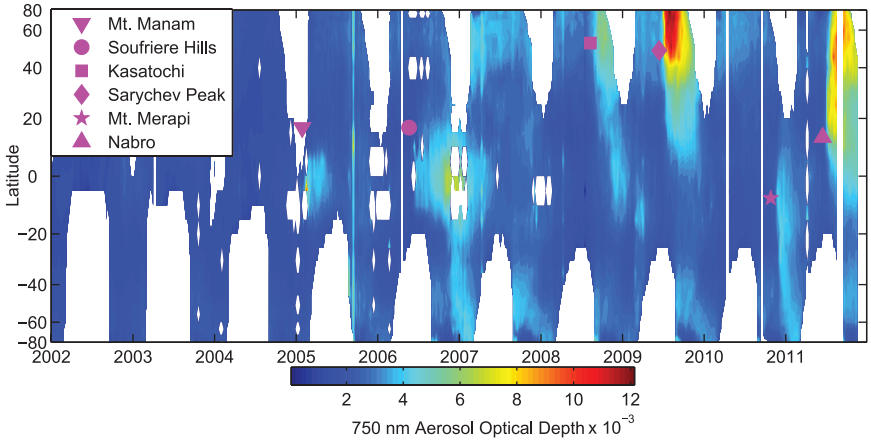

Fig. 1. The weekly zonal mean stratospheric aerosol optical depth at 750 nm for all measurements during the OSIRIS mission. The locations and times of the six volcanic eruptions with the largest stratospheric effect in the measurement record are noted with the markers. The yearly time label indicates 1 January of each year.

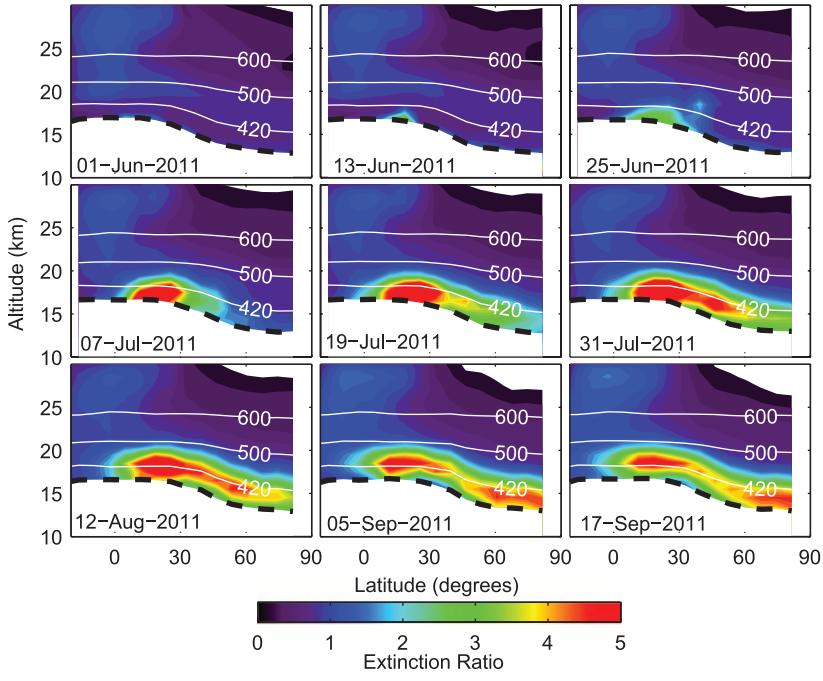

Fig. 2. Altitude profiles of the zonal average aerosol extinction ratio, over all longitudes, for 12-day time periods from June through September 2011, showing the progression of the stratospheric aerosol enhancement from the Nabro eruption on 13 June. The altitude of the 380 K level of potential temperature is shown by the dashed line with white contours (kelvin) for higher isentropic levels.

The OSIRIS instrument on the Odin spacecraft (*4*, *15*), launched in 2001, measures the spectrum of limb-scattered sunlight, providing vertical aerosol profiles and almost daily coverage of the sunlit globe. The measurements are used with a radiative transfer code to retrieve vertical profiles of stratospheric aerosol extinction coefficient at 750 nm (*16*, *17*). These agree with coincident SAGE III occultation measurements to within 10% during the 4 years of mission overlap, 2001 to 2005 (*18*). The time series of OSIRIS measurements of stratospheric aerosol optical depth over the past 10 years (Fig. 1) shows the large effect the recent Nabro eruption, 13 June 2011, had on the entire Northern Hemisphere, with zonal mean optical depths reaching some of the largest values in the entire OSIRIS record. The stratospheric aerosol optical depth is calculated for altitudes above 380 K potential temperature. The 380 K level corresponds to the altitude of the thermal tropopause in the tropics—typically 16 to 17 km—and is approximately the middle of the so-called tropical tropopause layer, or TTL (*19*). The use of this lower bound ensures that the optical depth shown is not due to tropospheric aerosol entering the lowermost stratosphere in the mid- and high latitudes, where air below the 380 K level and above the thermal tropopause can enter the stratosphere through quasi-horizontal isentropic transport. Optical depths above the background typical of the early OSIRIS years are also evident after earlier tropical volcanic eruptions, notably Mount Manam, January 2005; Soufrière Hills, May 2006; and Mount Merapi, October 2010. The northern high-latitude eruptions of Mount Kasatochi, August 2008, and Sarychev Peak, July 2009, both caused a notable effect on the stratospheric optical depth that extended to lower latitudes in the months after the eruption (*20*–*22*).

Tropical eruptions are particularly important to consider when analyzing global climate because stratospheric aerosol has a long lifetime in the tropical stratosphere and can be transported into the mid-latitudes of both hemispheres, as was the case with the Mount Manam eruption in 2005 and the Soufrière Hills eruption in 2006. In contrast, the volcanic aerosol enhancement from the Nabro eruption was largely confined to the Northern Hemisphere. The aerosol plume reached altitudes up to 21 km (Fig. 2), with rapid transport to higher latitudes following sloping isentropic levels. The maximum of the enhanced aerosol extinction ratio occurred at approximately 30°N latitude, substantially offset from the Nabro volcano at 13°N. There is a clear difference in the distribution of aerosol from Soufrière Hills and Nabro eruptions, which occurred within 3° of latitude and within 1 month in time of year of each other. The Soufrière Hills eruption reached altitudes of up to 20 km (*23*), which is well above the TTL, and the resulting aerosol circulated within the so-called tropical pipe, where mixing to mid-altitudes is weak (*24*, *25*). The Nabro eruption however, reached to much lower height and only attained stratospheric altitudes

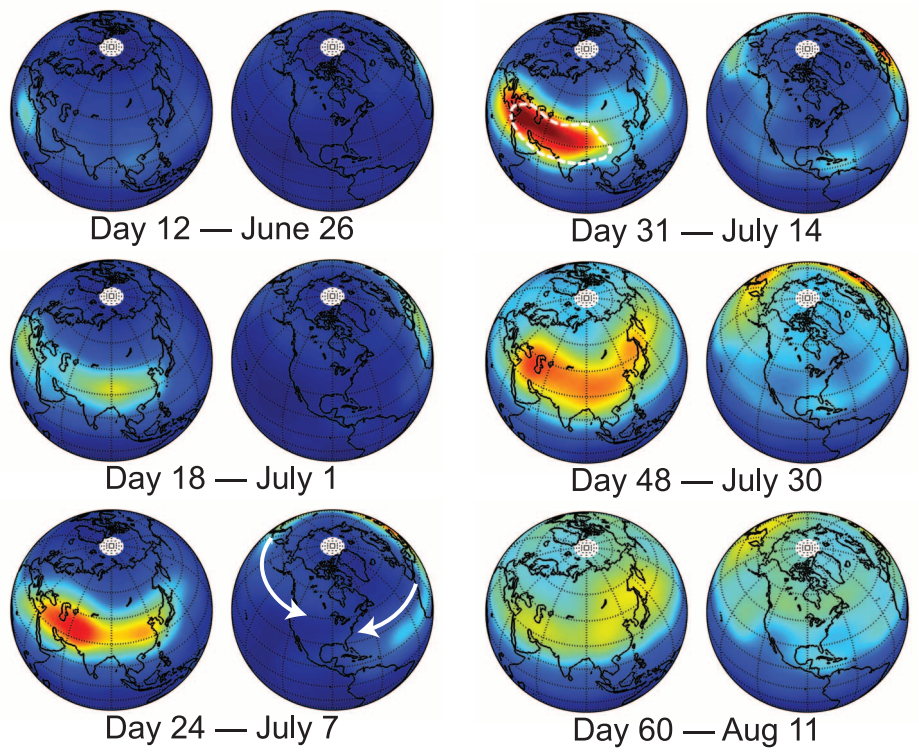

Fig. 3. Maps of the mean stratospheric aerosol optical depth at 750 nm for a series of selected days after the Nabro eruption. Each set of two maps, which are centered on Asia and North America, is a 5-day average, in which the day indicated is day 3 of the 5 days used in the average. White arrows indicate the direction of the plume transport. The dashed white line on the map for 14 July is a specific contour of geopotential height for 12 to 16 July that indicates the region of the Asian monsoon anticyclone (fig. S1).

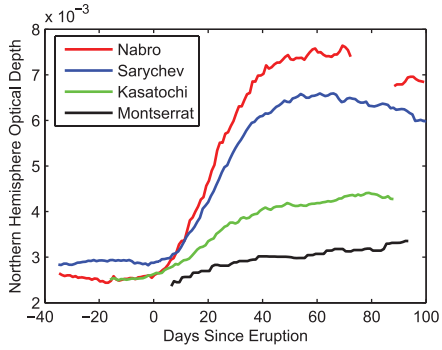

Fig. 4. The time series of Northern Hemisphere stratospheric aerosol optical depth during days after the volcanic eruptions that caused the four largest stratospheric perturbations as measured by OSIRIS since its launch in 2001. Soufrière Hills Montserrat (16.72°N, 62.18°W) erupted on 20 May 2006, Kasatochi (52.1°N, 175.3°W) erupted on 8 August 2008, and Sarychev (48.1°N, 153.2°E) began erupting on 12 June 2009. The reported SO_2 emissions of these eruptions were 1.3 Tg from Nabro (*3*), 1.2 Tg from Sarychev (*22*), 1.5 Tg from Kasatochi (*20*), and 0.1 Tg from Soufrière Hills Montserrat (*23*).

through subsequent transport processes associated with deep convection (fig. S3).

The history of stratospheric aerosol optical depth over the Northern Hemisphere (Fig. 3) shows that the aerosol enhancement built while remaining confined for several weeks to the region between central Asia and the Middle East. The zonal and meridional winds and geopotential height from the National Centers for Environmental Prediction (NCEP) at 200 and 100 hPa—approximately 13.5 AND 16.1 km, respectively (fig. S1)—show the strong Asian monsoon anticyclone, which existed from June through September over Asia and the Middle East, where the volcanic aerosol was observed. The monsoon anticyclonic vortex is known to provide an effective but slow vertical transport of tropospheric air to the stratosphere and confinement of the air in the lower stratosphere (*26*). For example, enhanced stratospheric hydrogen cyanide (HCN), measured by the Atmospheric Chemistry Experiment (ACE) satellite, are well correlated with the Asian monsoon region (*5*), and Cloud-Aerosol Lidar and Infrared Pathfinder Satellite Observations (CALIPSO) measurements have identified a coincident layer of enhanced aerosol concentrations (*7*). Vertical transport to stratospheric altitudes is particularly effective on the eastern side of the monsoon circulation (*26*), which is where a large stratospheric optical depth enhancement was first observed on 1 July, 18 days after the eruption (Fig. 3). At the same time, smaller but still enhanced optical depths were observed over North Africa, much closer to the Nabro eruption. CALIPSO measurements on 16 June show a large aerosol layer over North Africa at 10 to 13 km altitude colocated with a Global Ozone Monitoring Experiment-2 (GOME-2) observation of the SO_2 plume (fig. S2) and largely in good agreement with the reported eruption altitude. The NCEP winds at this level (fig. S1) are also consistent with the SO_2 plume dispersion; the plume is transported in the anticyclonic monsoon circulation from Africa to eastern Asia over a few days. CALIPSO measurements over both North Africa and the monsoon region on 1 July show extended aerosol layers at altitudes up to 20 km (fig. S3); the depolarization signature of these layers indicates spherical, presumably hydrated sulfate, aerosols originating from the volcanic SO_2. Together, these satellite measurements indicate rapid vertical transport of SO_2 through the TTL to the lower stratosphere. The deep convective activity associated with these geographic regions, which penetrates to approximately 17 km according to CALIPSO measurements (fig. S3), demonstrates that the rapid vertical transport of air by convection—largely thought to play a dominant role only below the TTL—can provide a rapid pathway to the stratosphere.

In later July, large values of optical depth were observed constrained to the region over Asia and the Middle East, until early August, when the enhanced aerosol dispersed and quickly circulated throughout the Northern Hemisphere, likely because of weakening of the anticyclone near the end of the monsoon. An interesting feature of the aerosol circulation was a small plume of westward transport at latitudes close to the equator and a second higher-latitude small plume undergoing eastward transport. These two plumes merged along the western side of North America on 14 July, 31 days after the eruption. In situ balloon measurements of stratospheric aerosol above Laramie, Wyoming (*27*), confirm the transport of volcanic aerosol over North America and provide estimates of particle size and concentration (fig. S4) at 46 and 140 days after the eruption.

A comparison of the evolution of daily Northern Hemisphere optical depth for the four largest volcanic eruptions in the OSIRIS record is shown in Fig. 4. The Northern Hemisphere optical depth is found by integrating the point measurements of optical depth for each day in a 2-week window over the hemispheric area. Peaking around 60 days after the eruption, the Nabro eruption is responsible for the largest stratospheric aerosol optical depth in the record and is approximately 15% larger than Sarychev, which was previously the largest. Given that the stratospheric aerosol burden was extremely low in the late 1990s and early 2000s because of the lack of any major volcanic eruptions, the Nabro eruption has caused the largest stratospheric aerosol burden since Mount Pinatubo. The impact of Nabro, a relatively low-altitude eruption, appears

to have been enhanced by its timing and location, allowing the Asian monsoon anticyclone to enhance the vertical transport while confining the majority of the aerosol to Asia and the Middle East until August, rather than rapidly mixing zonally and spreading throughout both hemispheres. The negative radiative forcing resulting from the 2011 Nabro eruption continues the trend from small eruptions of the past decade (*13*, *14*), but the inherently variable nature of volcanic eruptions means that any short-term future cooling of the surface from volcanic stratospheric aerosol is uncertain.

References and Notes

1. P. Hamill, E. J. Jensen, P. B. Russell, J. J. Bauman, *Bull. Am. Meteorol. Soc.* **78**, 1395 (1997).
2. Global Volcanism Program, Smithsonian Institution; http://www.volcano.si.edu/world/volcano.cfm?vnum=0201-101&volpage=weekly.
3. NASA Laboratory for Atmospheres, Science Highlights, July 2011; available at http://atmospheres.gsfc.nasa.gov/science/slides.php?sciid=9.
4. E. J. Llewellyn *et al.*, *Can. J. Phys.* **82**, 411 (2004).
5. W. J. Randel *et al.*, *Science* **328**, 611 (2010).
6. D. Hofmann, J. Barnes, M. O'Neill, M. Trudeau, R. Neely, *Geophys. Res. Lett.* **36**, L15808 (2009).
7. J.-P. Vernier, L. W. Thomason, J. Kar, *Geophys. Res. Lett.* **38**, L07804 (2011).
8. G. K. Yue, M. P. McCormick, E. W. Chiou, *J. Geophys. Res.* **96**, (D3), 5209 (1991).
9. M. P. McCormick, R. E. Veiga, *Geophys. Res. Lett.* **19**, 155 (1992).
10. M. P. McCormick, L. W. Thomason, C. R. Trepte, *Nature* **373**, 399 (1995).
11. E. G. Dutton, J. R. Christy, *Geophys. Res. Lett.* **19**, 2313 (1992).
12. A. Robock, *Rev. Geophys.* **38**, 191 (2000).
13. J.-P. Vernier *et al.*, *Geophys. Res. Lett.* **38**, L12807 (2011).
14. S. Solomon *et al.*, *Science* **333**, 866 (2011).
15. D. Murtagh *et al.*, *Can. J. Phys.* **80**, 309 (2002).
16. A. E. Bourassa, D. A. Degenstein, E. J. Llewellyn, *J. Quant. Spectrosc. Radiat. Transf.* **109**, 52 (2008).
17. A. E. Bourassa, D. A. Degenstein, R. L. Gattinger, E. J. Llewellyn, *J. Geophys. Res.* **112**, D10217 (2007).
18. A. E. Bourassa, L. A. Rieger, N. D. Lloyd, D. A. Degenstein, *Atmos. Chem. Phys.* **12**, 605 (2012).
19. S. Fueglistaler *et al.*, *Rev. Geophys.* **47**, RG1004 (2009).
20. B. Kravitz, A. Robock, A. E. Bourassa, *J. Geophys. Res.* **115**, D00L05 (2010).
21. A. E. Bourassa, D. A. Degenstein, B. J. Elash, E. J. Llewellyn, *J. Geophys. Res.* **115**, D00L03 (2010).
22. J. M. Haywood *et al.*, *J. Geophys. Res.* **115**, D21212 (2010).
23. A. J. Prata, S. A. Carn, A. Stohl, J. Kerkmann, *Atmos. Chem. Phys.* **7**, 5093 (2007).
24. C. R. Trepte, M. H. Hitchman, *Nature* **355**, 626 (1992).
25. R. A. Plumb, *J. Geophys. Res.* **101**, 3957 (1996).
26. M. Park, W. J. Randel, A. Gettelman, S. T. Massie, J. H. Jiang, *J. Geophys. Res.* **112**, D16309 (2007).
27. T. Deshler, M. E. Hervig, D. J. Hofmann, J. M. Rosen, J. B. Liley, *J. Geophys. Res.* **108**, 4167 (2003).

Acknowledgments: A.E.B., D.A.D., and E.J.L. are supported by the Natural Sciences and Engineering Research Council of Canada and the Canadian Space Agency. A.R. is supported by U.S. National Science Foundation (NSF) grant ATM-0730452. T.D. and the Wyoming in situ measurements are supported by NSF grant ATM-1011827. W.J.R. acknowledges support of the NASA Aura Science Team. The National Center for Atmospheric Research is sponsored by NSF. The authors thank the Keck Institute for Space Studies for providing a forum to discuss topics in this paper, and C. Roth and M. Park for help with creating the figures. OSIRIS data are publicly available at odin-osiris.usask.ca; CALIPSO data at http://eosweb.larc.nasa.gov/PRODOCS/calipso/table_calipso.html; GOME2 data at http://sacs.aeronomie.be/products.php; in situ balloon data at ftp://cat.uwyo.edu/pub/permanent/balloon/Aerosol_InSitu_Meas; and NCEP data at www.esrl.noaa.gov/psd/data/gridded/data.ncep.reanalysis.html.

Supplementary Materials

www.sciencemag.org/cgi/content/full/337/6090/78/DC1
Figs. S1 to S4

19 January 2012; accepted 11 May 2012
10.1126/science.1219371

ENSO Drove 2500-Year Collapse of Eastern Pacific Coral Reefs

Lauren T. Toth,[1] Richard B. Aronson,[1,2]* Steven V. Vollmer,[3] Jennifer W. Hobbs,[1] Dunia H. Urrego,[1,4] Hai Cheng,[5,6] Ian C. Enochs,[7,8] David J. Combosch,[3] Robert van Woesik,[1] Ian G. Macintyre[2]

Cores of coral reef frameworks along an upwelling gradient in Panamá show that reef ecosystems in the tropical eastern Pacific collapsed for 2500 years, representing as much as 40% of their history, beginning about 4000 years ago. The principal cause of this millennial-scale hiatus in reef growth was increased variability of the El Niño–Southern Oscillation (ENSO) and its coupling with the Intertropical Convergence Zone. The hiatus was a Pacific-wide phenomenon with an underlying climatology similar to probable scenarios for the next century. Global climate change is probably driving eastern Pacific reefs toward another regional collapse.

Global climate change is altering coral reef ecosystems through increasing sea temperatures and declining carbonate saturation states (*1*, *2*). Warmer and more acidic conditions inhibit coral calcification, carbonate precipitation, and submarine cementation (*3*–*5*). These effects are expected to reduce long-term rates of reef framework construction. Here we provide an explicit test of this prediction by showing how vertical reef accretion in the tropical eastern Pacific (TEP) responded to climatic oscillations during the Holocene. Increased variability of the El Niño–Southern Oscillation (ENSO) ~4000 years ago produced conditions in the TEP similar to those expected under plausible scenarios of future climate, stalling reef accretion off the Pacific coast of Panamá for 2500 years.

Living coral assemblages in the TEP respond to two principal environmental drivers: upwelling on a seasonal scale (*6*) and ENSO on a multiannual scale (*7*). The depressed water temperatures and reduced pH levels that accompany seasonal upwelling reduce coral growth (*6*). High sea temperatures associated with El Niño events cause bleaching, which reduces coral growth or kills corals outright (*7*). Mass coral mortality has been followed by intense bioerosion and the net loss of reef framework on a multidecadal scale (*8*). Upwelling and El Niño events are thought to account for generally poor Holocene reef development in the TEP (*6*, *7*, *9*), but neither has been explicitly linked to millennial-scale rates of reef accretion. We investigated the history of reef framework construction along an upwelling gradient in Pacific Panamá and evaluated the influences of seasonal upwelling and ENSO on the tempo and mode of reef development.

The uncemented reef frameworks of the TEP consist of coral fragments packed in fine sediment. We extracted 14 push-cores from subtidal reef-slope habitats on three reefs across Pacific Panamá with distinct upwelling regimes (*10*). Isla Contadora, in the Gulf of Panamá, experiences intense seasonal upwelling; upwelling is intermediate at Isla Iguana, also in the Gulf of Panamá; and there is no upwelling at Isla Canales de Tierra in the Gulf of Chiriquí

[1]Department of Biological Sciences, Florida Institute of Technology, 150 West University Boulevard, Melbourne, FL 32901, USA. [2]Department of Paleobiology, National Museum of Natural History, Smithsonian Institution, 10th and Constitution Avenue, NW, Washington, DC 20560, USA. [3]Marine Science Center, Northeastern University, 430 Nahant Road, Nahant, MA 01908, USA. [4]UMR-CNRS 5805 EPOC, Environnements et Paléoenvironnements Océaniques et Continentaux, Université Bordeaux 1, Avenue des Facultés, 33405 Talence, France. [5]Institute of Global Environmental Change, Xi'an Jiaotong University, Xi'an 710049, China. [6]Department of Geology and Geophysics, University of Minnesota, Minneapolis, MN 55455, USA. [7]Cooperative Institute for Marine and Atmospheric Sciences, Rosenstiel School of Marine and Atmospheric Science, University of Miami, 4600 Rickenbacker Causeway, Miami, FL 33149, USA. [8]Atlantic Oceanographic and Meteorological Laboratories, National Oceanic and Atmospheric Administration (NOAA), 4301 Rickenbacker Causeway, Miami, FL 33149, USA.

*To whom correspondence should be addressed. E-mail: raronson@fit.edu